FUEL PIN PRELIMINARY DESIGN

Nuclear Engineering – Politecnico di Milano

Simone Pagliuca, Tommaso Pirola, Lisa Raffuzzi, Riccardo Ronchi, Darien Shabi

simone1.pagliuca@mail.polimi.it

Course: Nuclear Design and Technologies
Academic year: 2024/2025

ABSTRACT: lorem ipsum dolor sit amet, consectetur adipiscing elit. Donec auctor, nunc nec ultricies ultricies, nunc nunc.

Key-words: Key, Words, Here

CONTENTS

1 INTRODUCTION

This report presents the preliminary design and verification of a fuel pin for a sodium-cooled fast reactor, as specified in the assignment.
The analysis involves calculations for material properties, thermal-hydraulic conditions, and mechanical stress limits.
We verify the robustness of our models and justify the assumptions made throughout the process.

1.1 Problem Description

The fuel pin design problem requires:

- Determining the cladding thickness, fuel-cladding gap size, and plenum height.
- Verifying the design against limits for fuel melting, cladding temperature, yielding, and rupture time.
- Identifying critical aspects if irradiation time is doubled.

The project specifications and material properties are mostly given, whenever we had missing information we either used data from previous the handouts which were provided and regarder a similar reactor, or we found the data from the literature.

1.2 Assumptions

To address the given problem, the following assumptions were made:

Steady State Solution for Gas in Grains:

↪ The rate equation for the gas remaining in the grains (PDE) was solved in steady state conditions, given that we just want to size the plenum for 1-year operation and are not interested in the specific behavior in time of the function.

Fission Rate Calculation:

↪ The fission rate was calculated by using the formula (macroscopic cross section * average flux).

↪ The macroscopic cross section of fission was computed from data taken from the JANIS database.

↪ The average flux was evaluated considering power and flux profile to be equal.

Material Properties and Geometry:

↪ Material properties are temperature-dependent and were modeled using provided empirical correlations.

↪ Axial power and neutron flux profiles remain constant over time.

↪ Initial helium pressure and temperature in the fuel-cladding gap were assumed as specified.

↪ Simplifications in geometry, such as neglecting axial deformation, were made to ease computation.

2 VERIFICATION OF MODELS

Each part of the analysis code has been checked to confirm it behaves as expected under the defined conditions.

2.1 Thermal-Hydraulics Analysis

Preliminary checks were conducted on coolant properties.

Density, viscosity, and thermal conductivity were validated at the coolant inlet temperature.

The heat transfer coefficient between the coolant and cladding was computed using Nusselt number correlations.

Figure 1 shows the axial power profile. the computed heat transfer coefficient in cold geometry was $\alpha_{coolant} = 139.98 \frac{kW}{m^2 K}$.

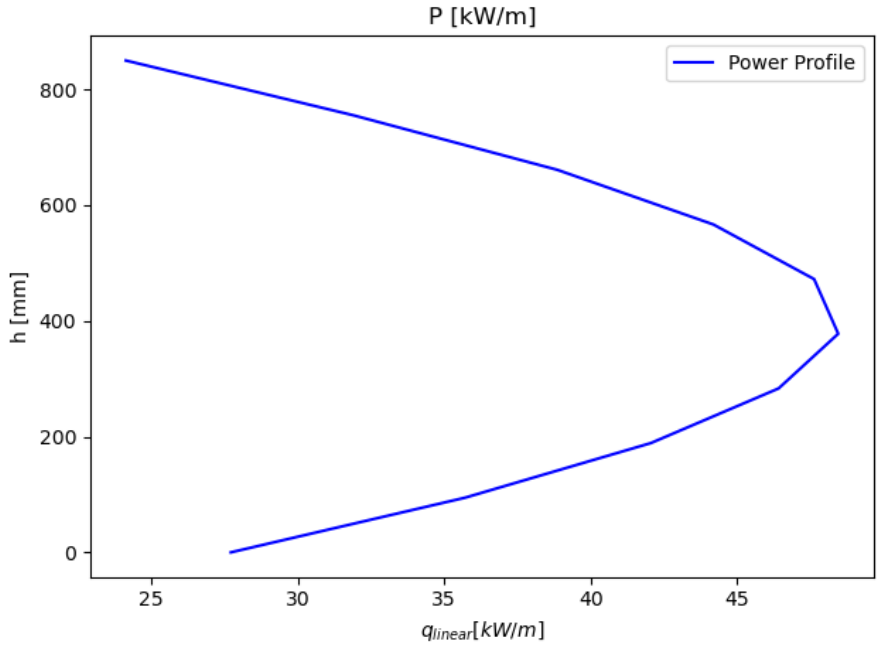

Figure 1: Thermal-hydraulics analysis results.

2.2 Temperature Profiles

Radial and axial temperature profiles were computed for the cold geometry to check if the shape of the profile made sense and if the values were reasonable.

We create a temperature map of the fuel rod. For every node along the axial direction, we first compute the temperature increase in the coolant due to the heat generated in the fuel. From this we compute the temperature at the coolant cladding interface using the heat transfer coefficient (computed by given correlations). For the cladding again we approximate to a linear temperature profile and compute the temperature at the cladding gas interface. Then for the gap and the fuel we compute several temperature points along the radius, at every step the properties are updated to the temperature of the previous step. The inner void is at the same temperature as the inner surface of the fuel.

The results provided an initial validation of the temperature distribution behavior before further analysis.

Figure 2 illustrates the temperature along the axis, at the interfaces, while Figure 3 shows the radial temperature profiles at the bottom, middle and top of the fuel rod.

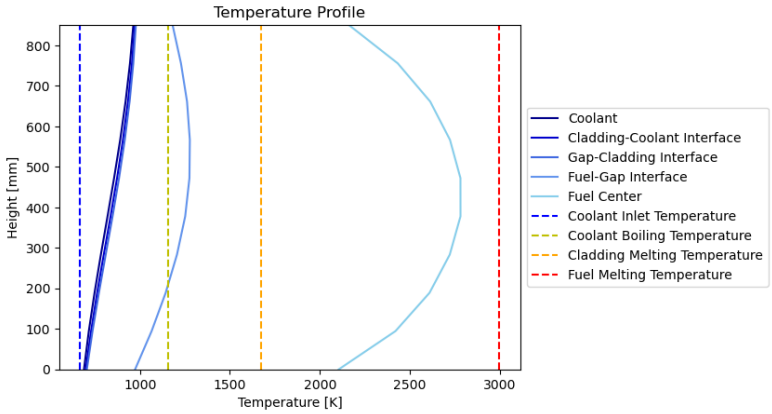

Figure 2: Axial temperature profile for cold geometry.

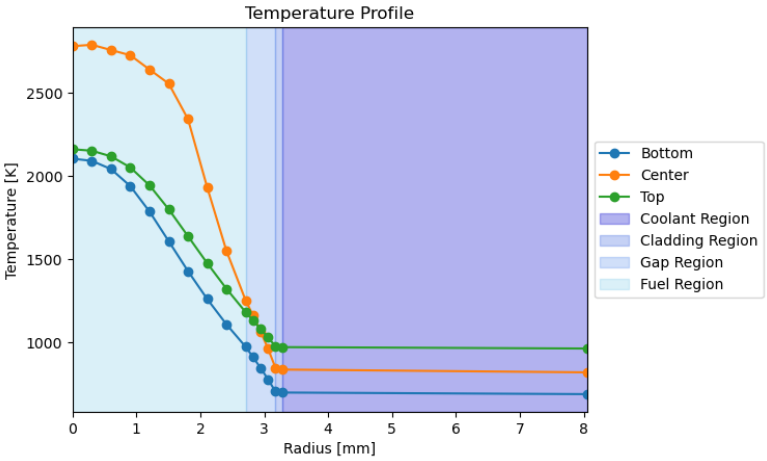

Figure 3: Radial temperature profile for cold geometry.

2.3 Thermal Expansion Analysis

The fuel and cladding form a coupled system, with the gap between them playing a crucial role in heat transfer, mechanical interactions, and safety. Accurate evaluation of thermal expansion is essential to ensure efficient operation and structural integrity of the reactor core. The calculations consider material-specific thermal expansion coefficients and the temperature distributions derived from reactor operational data.

2.3.1 Axial Temperature Profile of the Fuel and Axial Profile of Fuel Radius (Cold vs. Hot Geometry)

The fuel's axial temperature profile under hot operational conditions is shown in Figure 4. It illustrates the temperature distribution along the fuel height, which is essential for understanding thermal stresses and expansion. We can see that the material's expansion follows perfectly the fuel temperature profile (Figure 5).

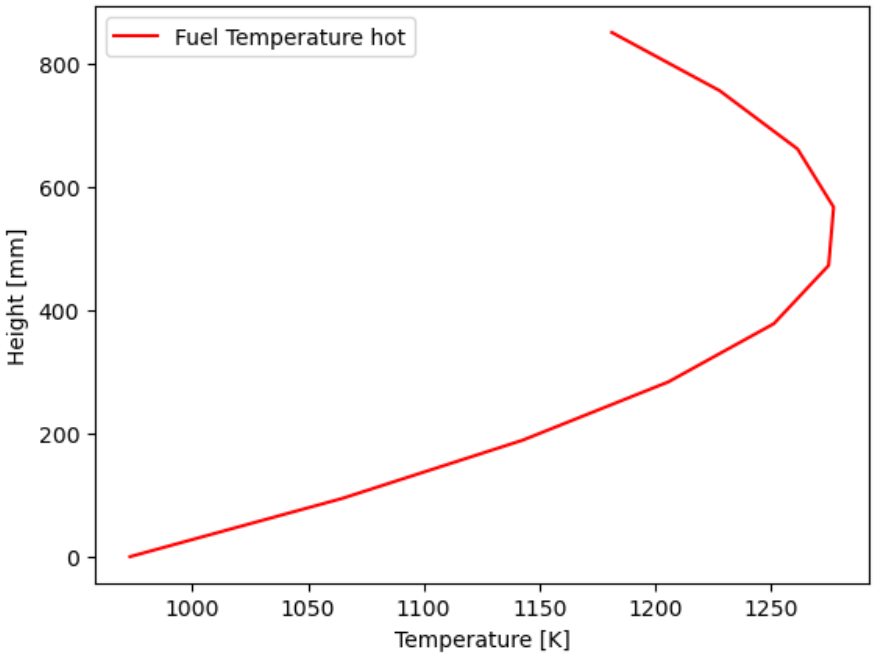

Figure 4: Axial temperature profile of the fuel under hot conditions.

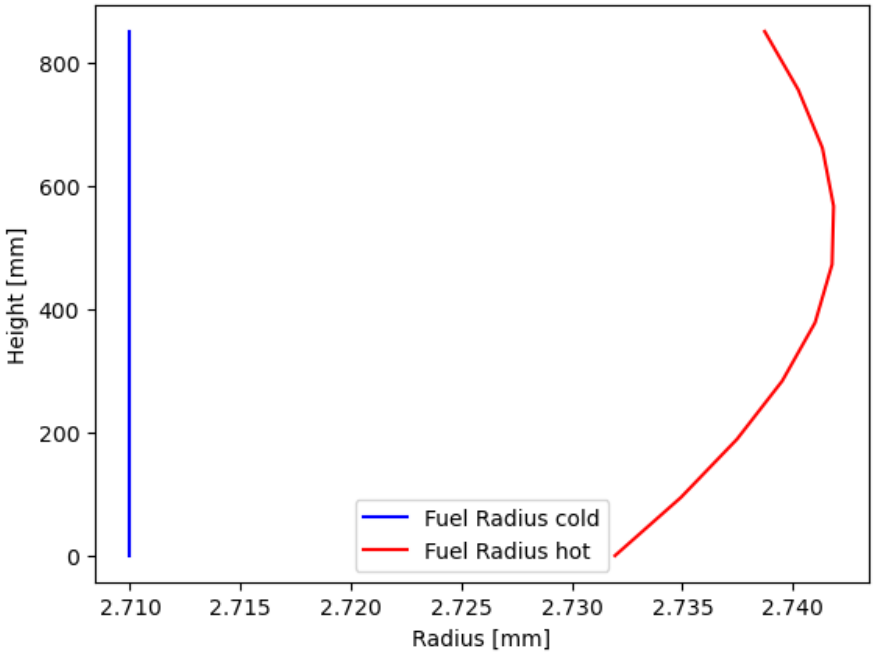

Figure 5: Axial profile of fuel radius (cold vs. hot geometry).

2.3.2 Axial Temperature Profile of the Inner and Outer Cladding (Cold vs. Hot Geometry)

The inner and outer temperature profiles of the cladding show the thermal distribution along its axial height. These graphs highlight the uniform expansion of the cladding along its height (Figure 6). The temperature difference between the inner and outer part is uniform, as shown in Figure 7.

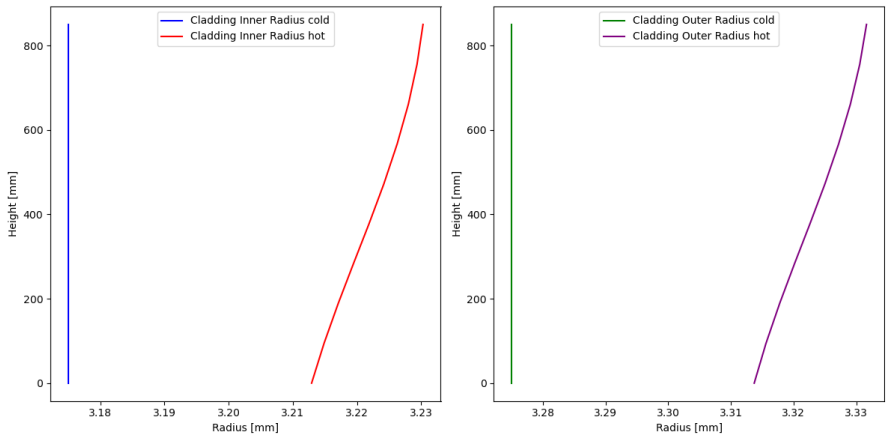

Figure 6: Axial temperature profile of the cladding (cold vs. hot geometry).

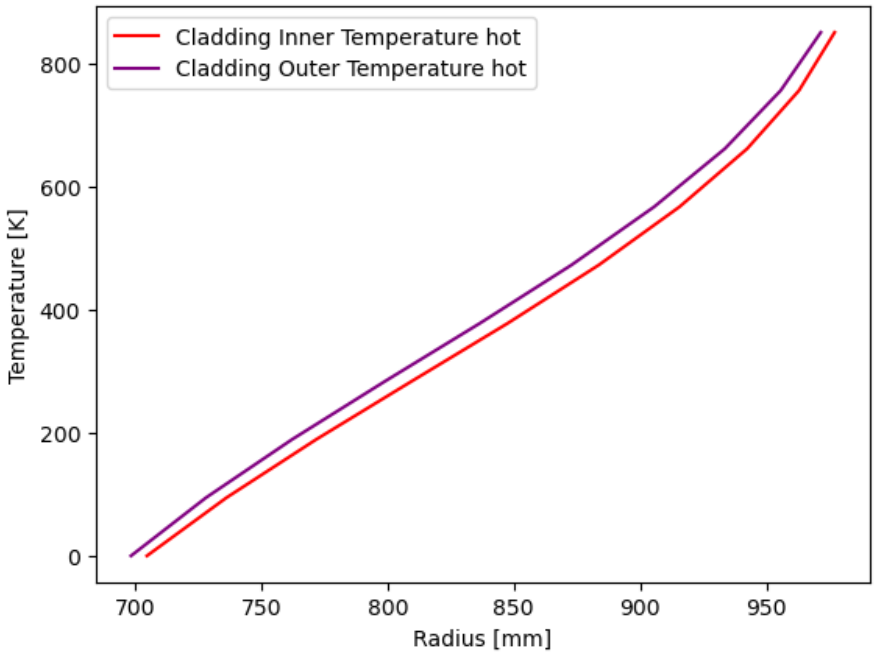

Figure 7: Axial profile of cladding radius (cold vs. hot geometry).

2.3.3 Gap and Cladding Thickness Along Axial Height

The evolution of the fuel-cladding gap due to differential expansion is shown in Figure 8. This parameter directly impacts heat transfer efficiency and mechanical interactions in the reactor core. The change in cladding thickness with temperature is minimal compared to the change in radius. However, it is still a key parameter for evaluating structural integrity.

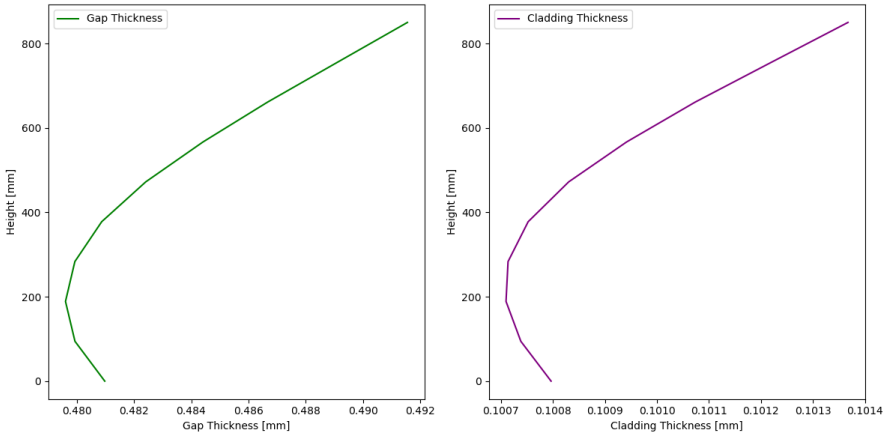

Figure 8: Gap and cladding thickness along the axial height.

2.3.4 Discussion

As expected, the fuel's thermal expansion is more pronounced due to its higher temperature gradient compared to the cladding. The gap between the fuel and cladding decreases, which improves thermal coupling but must be managed carefully to avoid mechanical interactions that could compromise the system's integrity.

2.4 Void Swelling

A correlation for the volumetric void swelling of the cladding was given. We assumed the swelling to be isotropic and therfore the radial expansion is $\frac{1}{3}$ of the volumetric expansion. Figure 9 shows the swelling of the cladding along the axial direction. We can see that, as expected, the swelling is only contained within a range of temperature: too low and no swelling, too high and the mobility is high enough that recombination prevails.

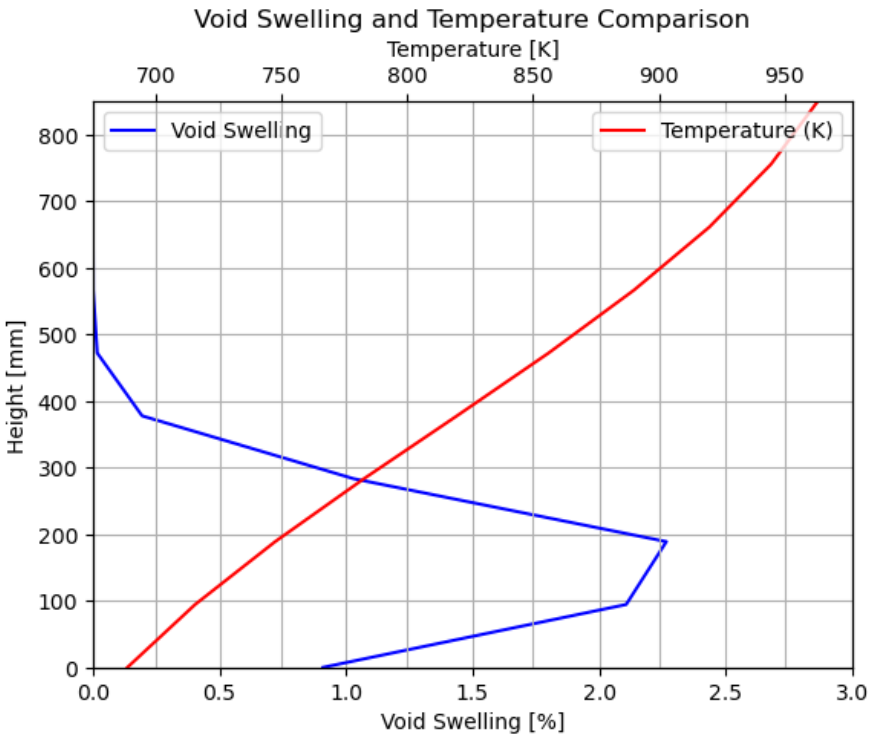

Figure 9: Cladding swelling due to void formation.

3 FISSION GAS BEHAVIOUR

In this section, the behaviour of the two main gases produced by fission events (Xenon and Krypton) is addressed, with particular focus on the impact of this phenomenon on some design parameters, such as the height of the plenum.

Both Xe and Kr are chemically inert gases, with a combined fission yield around 30% (this value includes even other fast-decay fission products, which will result in Xe and Kr within few minutes).

Due to fission events, there will be a constant production rate of fission gas atoms, distributed in the fuel, giving rise to two main phenomena: Fuel Gaseous Swelling and Fission Gas Release.

3.1 Fission Gas Release

Due to essentially diffusion, part of the gas created in the fuel will be released in the plenum. Xe and Kr will "pollute" the He initially contained in the plenum, decreasing its thermal conductivity and increasing the internal pressure of the pin (additional moles of gas are being introduced in a fixed volume).

All these phenomena are always ongoing under irradiation and affect the thermo-mechanical behaviour of the fuel pin in a highly non-linear way. It is crucial, then, to be able to correctly predict and control them.

The problem is tackled through the Rate Theory Equations, coupled with some Cluster Dynamics considerations. The physics of the phenomenon is described at the grain scale, which is taken as the domain for the problem. The equations to solve are essentially two:

The equation to estimate the total amount of gas that is produced, a simple ODE:

$$\frac{dP}{dt} = y \cdot \dot{F} \quad \text{with} \quad \begin{cases} P\left(\frac{\text{at}}{\text{m}^3}\right) : \text{gas produced} \\ y : \text{fission yield (combined)} \\ \dot{F} : \text{fission rate} \end{cases} \tag{1}$$

The equation for the intra-granular behaviour of gases, merging the gas remaining in solution and the gas held inside bubbles in a single term named G_M, indicating the gas retained by the fuel grain itself:

$$\frac{dG_M}{dt} = D_{\text{eff}} \cdot \nabla^2 G_M + y \cdot \dot{F} \quad \text{with} \quad \begin{cases} G_M\left(\frac{\text{at}}{\text{m}^3}\right) : \text{gas retained by grain} \\ D_{\text{eff}} : \text{effective diffusivity (embeds all the phenomena)} \end{cases} \tag{2}$$

3.2 Main Assumptions, Data, and Hypotheses

- Domain size: grain size $d_g = 10\,\mu$m.
- The reference model for diffusivity is the one by Matzke, 1980:

$$D_{\text{eff}}[\text{m}^2/\text{s}] = D_0 \cdot \exp\left(-\frac{Q}{T}\right) \tag{3}$$

$$\text{with } D_0 = 5 \cdot 10^{-8}\,\text{m}^2/\text{s}, \quad Q = -40262, \quad T\,[\text{K}] = \text{temperature} \tag{4}$$

- The reference temperature T_{ref} considered is the simple average of the three main axial temperatures at the centre of the fuel (first "slice", midplane, last "slice"). This is a conservative hypothesis, as diffusivity is enhanced by high temperatures and the temperatures at the inner radius are the highest.
- The fission yield considered is the combined Xe and Kr one: $y = 30\%$.
- The fission rate is computed through the expression:

$$\dot{F} = \Sigma_f \cdot \phi_{\text{avg}} \tag{5}$$

  Where the global macroscopic fission cross section is obtained combining the microscopic cross sections for all the isotopes in the analysed fuel configuration (see reference for cross-section data), and the average neutron flux is computed assuming an axial profile equivalent to the one for linear power, through a "peak-to-average" factor.
- Initial conditions: $P(0) = 0; G_M(0) = 0$.
- Boundary conditions for G_M (Booth, 1957):
  - "Zero" boundary at surface (perfect sink): $G_M(a) = 0$
  - Symmetry at the centre: $\frac{dG_M(0)}{dr} = 0$

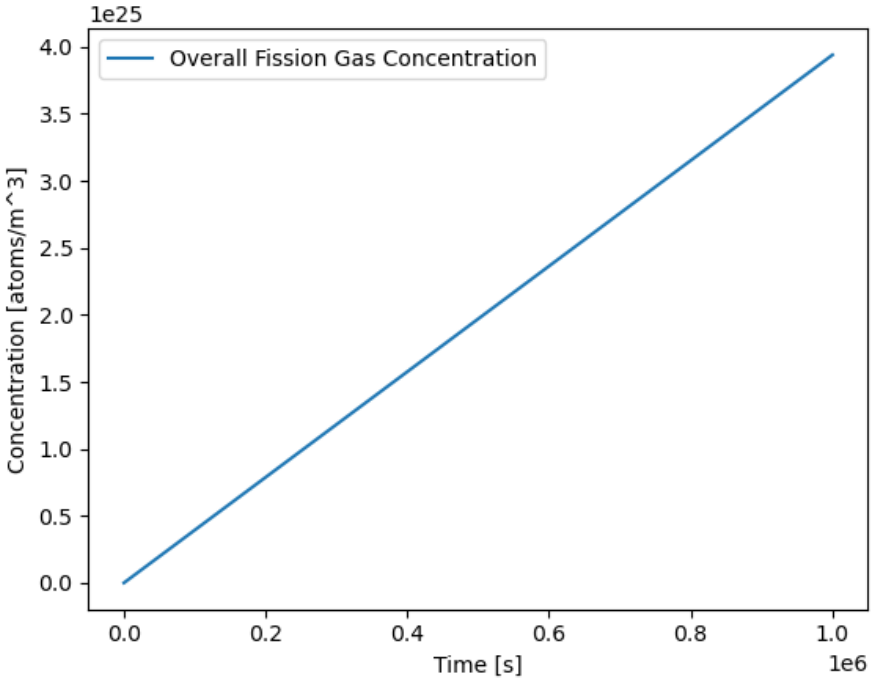

Figure 10: Fission Gas Release dynamics and intra-granular behaviour of G_M.

- The solution would generally look like:
- The gas released is, then, the difference between the two shown quantities.
- As the timescale of the phenomenon is very small (fast) and the design must be targeted to one year of operation (360 effective days), the behaviour of the G_M can be reasonably considered stabilized to the steady-state solution.
  The simplifying assumption made is then to neglect the time derivative in the equation, solving and integrating the simple remaining ODE on the specified domain.
- This model is considered suitable for describing the situation after the incubation time, which is neglected.

3.3 Results and Comments

3.3.1 Total Gas Produced

Here the actual solution for the fission gas production equation:

$$\frac{dP}{dt} = Y_f \cdot \dot{F} \tag{6}$$

By computing the value at $t = 360$ days, the total gas produced is obtained.

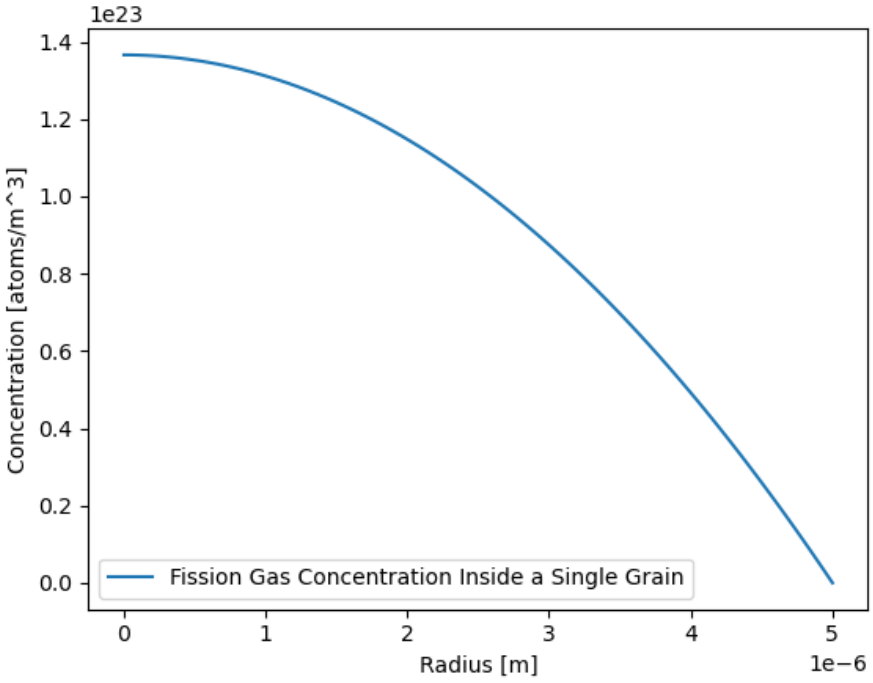

Figure 11: Fission Gas Release over operational time.

3.3.2 Gas Retained by Grain

By solving the G_M equation, the following spatial distribution is found:

Integrating this curve in the whole domain (grain size) and multiplying the obtained value for the number of grains in a fuel pellet (considered to be 10^5) and the number of fuel pellets for each pin, the total amount of fission gas retained in the fuel is evaluated.

The total FGR is then the difference between the two quantities. Here the summary of the computed parameters and quantities:

Table 1: Summary of Computed Parameters and Quantities

Parameter	Value
Σ_f	0.027 cm^{-1}
ϕ_{avg}	$4.87 \cdot 10^{15}$ n/$cm^2 \cdot$ s
$\dot{F}$	$1.31 \cdot 10^{20}$ fissions/$m^3 \cdot$ s
T_{avg}	2349.25 K
D_{eff}	$1.8 \cdot 10^{-15}$ m^2/s
$P(1y)$	$1.23 \cdot 10^{27}$ at/m^3
$G_M(1y)$	$1.10 \cdot 10^{25}$ at/m^3
FGR	$1.21 \cdot 10^{27}$ at/m^3

N.B. Considering the orders of magnitude, a wise simplification would have been to directly neglect the gas retained in the grain and assume the totality of the gas produced as immediately released in the plenum. This hypothesis is also supported by the very high temperature

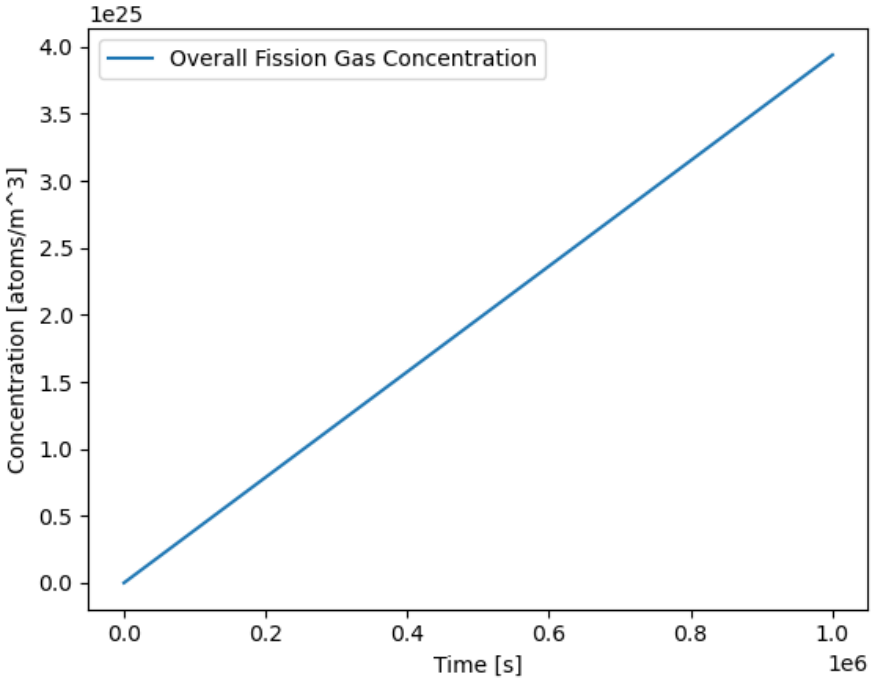

Figure 12: Overall Fission Gas Concentration

characterizing the problem.

3.4 Impact on the Design

The FGR will increase the internal pressure of the fuel pin. Although it is not a major concern regarding the interaction with the coolant (which is almost at atmospheric pressure), it may be an issue for the stainless-steel cladding mechanical behaviour. Too high internal pressure would result in the cladding being too much under tension, affecting its mechanical properties.

To avoid very strong effects on the cladding, a limit on the internal pressure of the pin is set to 5 MPa.

Considering the height of the plenum fixed, it is then possible to evaluate the new pressure of the filling gas (now "polluted") by a simple application of the ideal gas law:

$$p \cdot V = n \cdot R \cdot T \tag{7}$$

in which n will increase (release of new gas) and the temperature is considered to be locked to the initial value for the filling gas (20°C).

By considering a set of possible plenum heights, the acceptable ones will be leading to new internal pressure below the just cited limit.

As already mentioned, FGR will impact also on the thermal conductivity of the filling gas of the gap by reducing it. The conductivity worsening will lead to an increase in the fuel temperature. As diffusion processes are, in fact, temperature-driven, this will result in a higher Fission Gas Release.

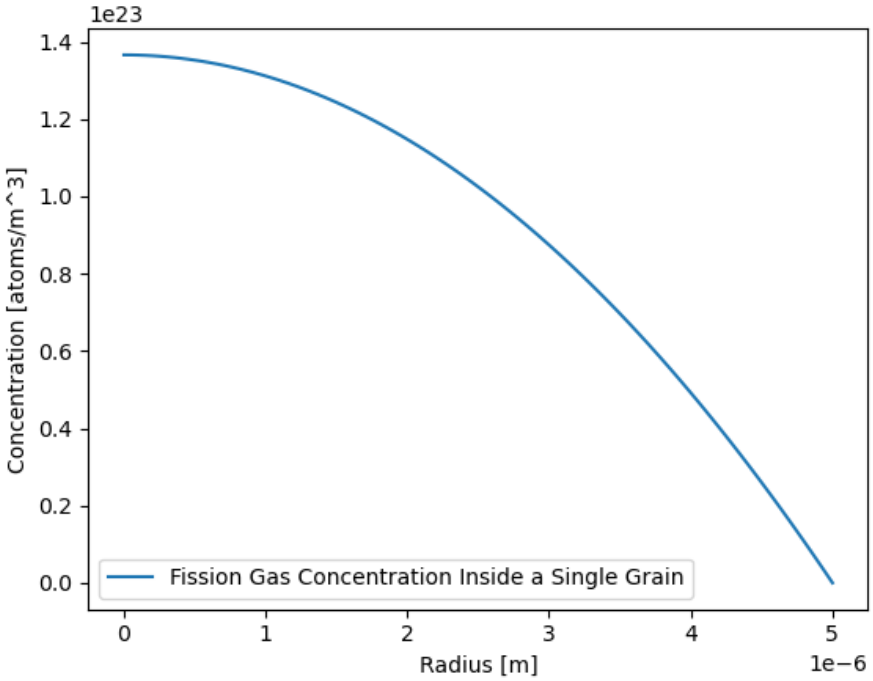

Figure 13: Fission Gas Concentration Inside a Single Grain

The designer will then have to deal with a "positive feedback" phenomenon, eventually stopped and stabilized by thermal expansion effects.

For this reason, both phenomena are considered in sequence, with an iterative calculation logic, to reach convergence with some specific temperature and FGR values.

3.5 Restructuring

After transitioning from cold geometry to hot geometry and evaluating the thermal expansion we have to take in account the fuel restructuring process. We make some assumption about columnar and equiaxed region-radii, as well as on densities in different regions. We set the temperature boundaries for columnar ragion at 1800°C and at 1600°C for equiaxed region, according to Holander's book. Regarding the densities, we consider that in the As-fabricated region the density remains the same, while in the equiaxed a percentage of TD of 95First of all, we evaluate columnar and equiaxed radii respectively at 1800°C and 1600°C as we said, based on a temperature map. This map provides the temperature at different heights along the fuel pin, using a precise function that allows us to determine the temperature at any position in the 3D model previously developed Once columnar and equiaxed radii are determined, we have to evaluate the void radius. The As-fabricated region is only the remaining potion of the fuel outer radius after subtracting the equiaxed region. Using this simple correlation to make a possible solution of void formation:

$$R_{void} = \sqrt{R_{\text{col}}^2 - R_{\text{eq}}^2 \cdot \left(\frac{\text{Density}_{\text{AS}}}{\text{Density}_{\text{col}}}\right) + \left(R_{\text{eq}}^2 - R_{\text{col}}^2\right) \cdot \left(\frac{\text{Density}_{\text{eq}}}{\text{Density}_{\text{AS}}}\right)} \tag{8}$$

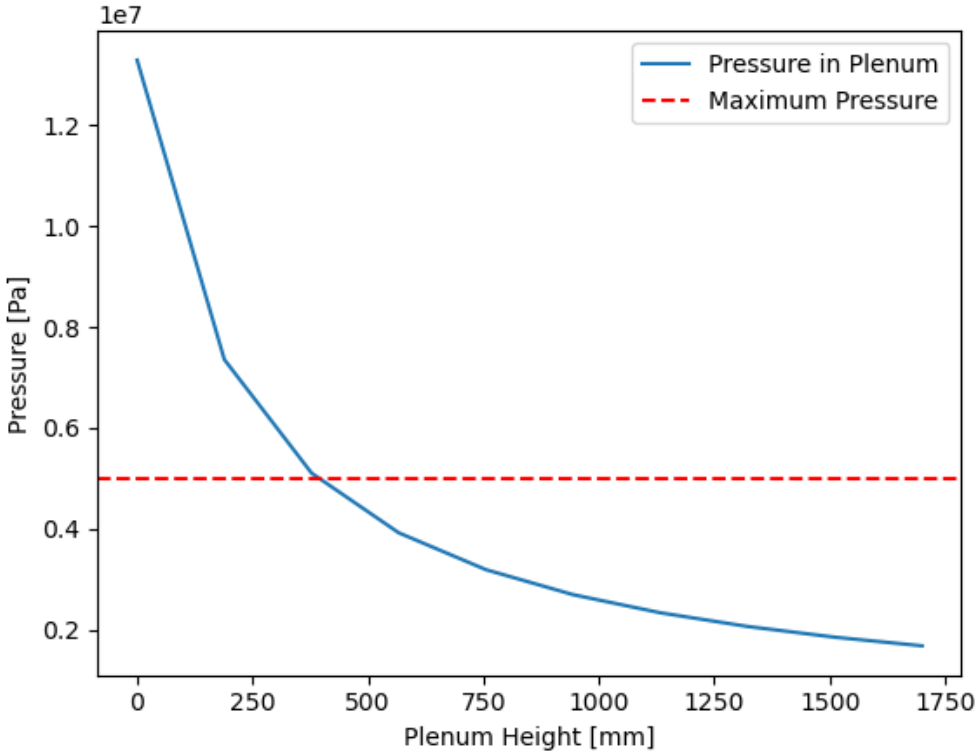

Figure 14: Pressure in Plenum vs Plenum Height

At end, there is the plot of the fuel element: height vs Radius. We want to show the restructuring phenomenon and highlight the contributions' dependence on the axial position-z of the fuel pin Figure 15 shows

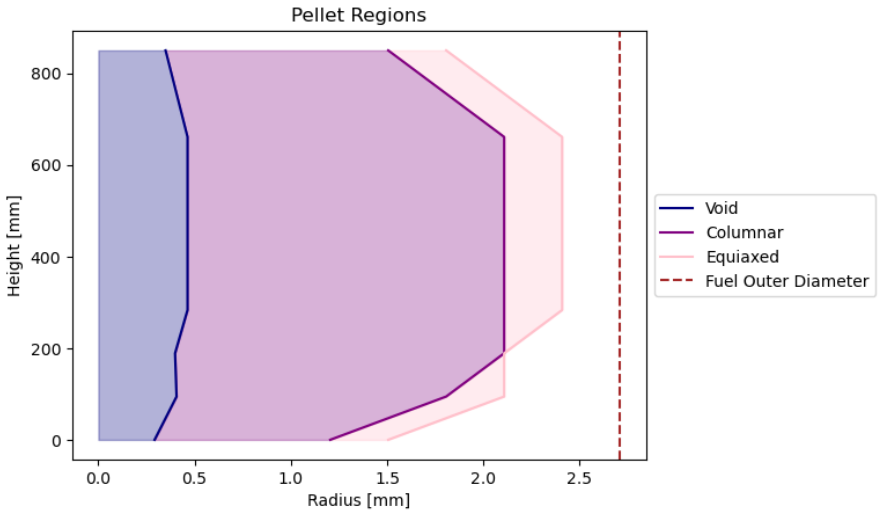

Figure 15: Cladding swelling due to void formation.

3.6 Stress Analysis

4 MECHANICAL ANALYSIS – STRESS ASSESSMENT

4.1 Introduction

The mechanical analysis focuses on evaluating the stresses in the cladding to ensure it remains within safe limits during operation. Stresses were computed using the Mariotte and Lamé criteria, the potential for plastic strain was assessed, and the time to rupture due to thermal creep was evaluated.

4.2 Methodology

The cladding stress distribution was computed using elasticity equations for cylindrical geometries:

- **Mariotte Criterion:**
  - Evaluates hoop stress at the mid-wall of the cladding.
  - Used to check for yielding. In preliminary calculations, the Mariotte stress was found to be slightly higher than the Lamé stress, though the latter criterion is more restrictive.
- **Lamé Criterion:**
  - Considers radial, hoop, and axial stresses.

  - Maximum stress differences are used to ensure compliance with yield and ultimate strength limits. The Lamé criterion was found to impose stricter limits (~33% more restrictive) compared to the Mariotte criterion.

- **Plastic Strain Check:**
  - Plastic strain is flagged if either criterion indicates stresses beyond the yield strength.
  - No significant plastic strain was observed when both criteria were satisfied.

- **Thermal Creep (Time to Rupture):**
  - The Larson-Miller Parameter (LMP) was used to compute the rupture time based on operating stresses and temperatures.
  - Even in conservative scenarios, the calculated time to rupture confirmed sufficient margins, indicating minimal risk of creep-related failure.

4.3 Results and Conclusion

Preliminary verification shows that the cladding meets safety requirements:

- **Stresses from Mariotte and Lamé:**
  - Both criteria confirmed that the stresses remain below critical limits.
  - While the Mariotte stress tends to be marginally higher, it is still within safe bounds. Lamé's stricter limits ensure additional safety.

- **Plastic Strain:**
  - No significant plastic strain was observed, indicating that the cladding will remain in the elastic regime under the specified operational conditions.

- **Time to Rupture:**
  - Using the LMP approach, the time to rupture due to thermal creep was calculated.
  - Even in the most conservative cases, the cladding demonstrated an operational life far exceeding the irradiation period.

These checks validate the cladding's mechanical reliability in the initial design. The preliminary analysis indicates that the proposed design is safe and robust, with sufficient margins for long-term operation. Further detailed evaluations can refine these results as the design evolves.

5 OTHER EFFECTS

Additional phenomena, such as plutonium redistribution and helium embrittlement, are considered to provide a broader understanding of the fuel pin's behavior.

5.1 Plutonium Redistribution

As a consequence of restructuring, it became necessary to investigate the phenomenon of Plutonium redistribution. During restructuring, as observed, the formation of distinct zones occurs within the fuel element:

- Central void
- Columnar grains (pores migrate, and mass is displaced outward)
- Equiaxed grains (caused by grain growth at high temperatures)
- As-fabricated (temperature is too low to cause changes)

These different zones are characterized by differences in density and, consequently, porosity. This is due to the densification of the fuel, reaching up to 98-99% of TD.

Due to this phenomenon, the density variation results in a change in Plutonium concentration across the different zones of the fuel, which initially had a uniform concentration of 29%. There is an enrichment of Plutonium in the central (columnar) zone, followed by an initial decrease reaching a minimum value, which corresponds to a depletion in the equiaxed zone. In the as-fabricated zone, the concentration stabilizes back to the initial value. The redistribution of Plutonium thus affects part of the fuel element and is a consequence of the high activation energy of Plutonium.

To evaluate how Plutonium redistribution varies following the phenomena of thermal expansion and fuel restructuring, we used the following formula, as provided in the handouts (Hot Effects Analysis, V):

$$\frac{q'''(r)}{q_0} = \frac{c(r)}{c_0} = 1 + D\left\{\exp\left[-2\alpha\left(\frac{r-r^*}{R_{\text{fo}}}\right)\right] - 2\cdot\exp\left[-\alpha\left(\frac{r-r^*}{R_{\text{fo}}}\right)\right]\right\} \tag{9}$$

where:

- $D = 0.01$ (from handouts),
- α is equal to 10 (from handouts),
- r^* is an empirical constant set to $0.207 \cdot R_{\text{fo}}$, a value that ensures the conservation of Plutonium during redistribution,
- $C(r)$ is the radial Plutonium concentration [g/cm^3],
- c_0 is the initial Plutonium concentration.

Graphically, this result clearly illustrates all the phenomena associated with Plutonium redistribution.

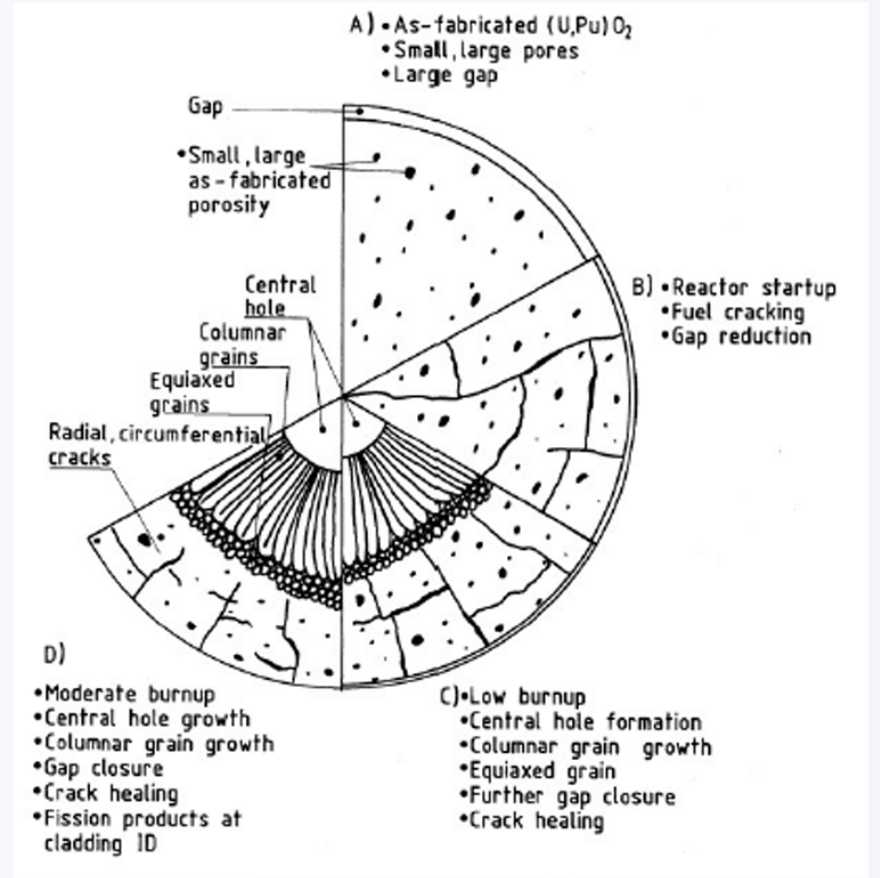

Figure 16: Restructuring of fuel elements and formation of zones during irradiation.

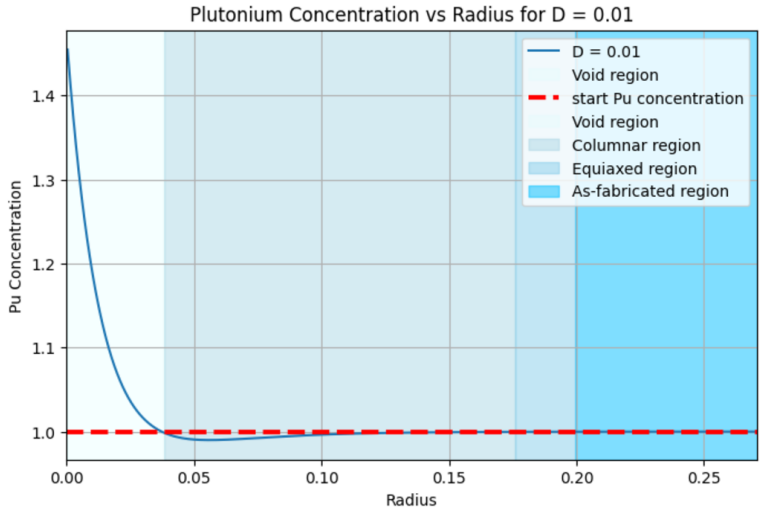

Figure 17: Radial distribution of Plutonium concentration (relative to starting concentration) within the fuel structure.

5.2 Helium Embrittlement

Figure 18 shows the swelling of the cladding along the axial direction.

Figure 18: Cladding swelling due to void formation.

6 DESIGN RESULTS AND CONCLUSION

The study presents the design outcomes, their implications, and the conclusions drawn on the feasibility and safety of the proposed design.

6.1 Code

After the verification process the different pieces of code had to be adapted to properly work toghether, the result of this was compared to the previous work to ensure that nothing was "corrupted" during the process.
We have then created a code that takes as input a value of cladding thickness and plenum height and will iterativly undergo the computation until the temperature map converges to a stable solution.
To dimensition these two quantities a previously implemented genetic algorithm was used.

6.2 Findings and Considerations

During the dimensioning process, it was observed that cladding thickness is highly dependent on the operational time specified in the fitness function. For short cycles, such as one year, the algorithm suggests a thinner cladding, which may not be suitable for long-term operation. Therefore, even when tasked with a one-year design, we opted to base the dimensioning on an expected four-year fuel cycle, which is more representative of fast reactor operation.

This conservative approach ensures greater reliability and safety margins over the lifecycle of the fuel pin. Additional findings and considerations will be added as further analyses are completed.

6.3 Results

The design and verification process confirmed that all key parameters remain well within the specified limits.
The finalized design dimensions are:

- **Cladding Thickness:** [Insert value here].
- **Plenum Height:** [Insert value here].

All of the code can be found in the following Github repository: https://github.com/simo-pagliu/NDT-Homeworks